

Effect of heating time on structural, morphology, optical, and photocatalytic properties of g-C_3N_4 nanosheets

Nguyen Manh Hung, Le Thi Mai Oanh, Lam Thi Hang, Pham Do Chung, Pham Thi Duyen, Dao Viet Thang, Nguyen Van Minh

Citation: Chin. Phys. B . 2020, 29(5): 057801 . **doi:** 10.1088/1674-1056/ab7e95
Journal homepage: http://cpb.iphy.ac.cn; http://iopscience.iop.org/cpb

What follows is a list of articles you may be interested in

Photoluminescence in fluorescent 4H-SiC single crystal adjusted by B, Al, and N ternary dopants

Shi-Yi Zhuo(卓世异), Xue-Chao Liu(刘学超), Wei Huang(黄维), Hai-Kuan Kong(孔海宽), Jun Xin(忻隽), Er-Wei Shi(施尔畏)
Chin. Phys. B . 2019, 28(1): 017101 . **doi:** 10.1088/1674-1056/28/1/017101

Investigations on mesa width design for 4H-SiC trench super junction Schottky diodes

Xue-Qian Zhong(仲雪倩), Jue Wang(王珏), Bao-Zhu Wang(王宝柱), Heng-Yu Wang(王珩宇), Qing Guo(郭清), Kuang Sheng(盛况)
Chin. Phys. B . 2018, 27(8): 087102 . **doi:** 10.1088/1674-1056/27/8/087102

Effect of pressure on the elastic properties and optoelectronic behavior of $Zn_4B_6O_{13}$: First-principles investigation

Pei-Da Wang(王培达), Zhen-Yuan Jia(贾镇源), Yu-Han Zhong(钟玉菡), Hua-Yue Mei(梅华悦), Chun-Mei Li(李春梅), Nan-Pu Cheng(程南璞)
Chin. Phys. B . 2018, 27(5): 057101 . **doi:** 10.1088/1674-1056/27/5/057101

Passivation of carbon dimer defects in amorphous SiO_2/4H-SiC (0001) interface: A first-principles study

Yi-Jie Zhang(张轶杰), Zhi-Peng Yin(尹志鹏), Yan Su(苏艳), De-Jun Wang(王德君)
Chin. Phys. B . 2018, 27(4): 047103 . **doi:** 10.1088/1674-1056/27/4/047103

The residual C concentration control for low temperature growth p-type GaN

Shuang-Tao Liu(刘双韬), De-Gang Zhao(赵德刚), Jing Yang(杨静), De-Sheng Jiang(江德生), Feng Liang(梁锋), Ping Chen(陈平), Jian-Jun Zhu(朱建军), Zong-Shun Liu(刘宗顺), Xiang Li(李翔), Wei Liu(刘炜), Yao Xing(邢瑶), Li-Qun Zhang(张立群)
Chin. Phys. B . 2017, 26(10): 107102 . **doi:** 10.1088/1674-1056/26/10/107102

Effect of heating time on structural, morphology, optical, and photocatalytic properties of g-C_3N_4 nanosheets*

Nguyen Manh Hung[1,4], Le Thi Mai Oanh[1,2,†], Lam Thi Hang[1,3], Pham Do Chung[2], Pham Thi Duyen[1,5], Dao Viet Thang[1,4], and Nguyen Van Minh[1,2]

[1] *Center for Nano Science and Technology, Hanoi National University of Education, 136 Xuan Thuy Road, Cau Giay District, Hanoi, 100000, Vietnam*
[2] *Department of Physics, Hanoi National University of Education, 136 Xuan Thuy Road, Cau Giay District, Hanoi, 100000, Vietnam*
[3] *Faculty of Basic Sciences, Hanoi University of Natural Resources and Environment, 41A Phu Dien Road, North Tu Liem, Hanoi, 100000, Vietnam*
[4] *Hanoi University of Mining and Geology, Duc Thang ward, North Tu Liem District, Hanoi, 100000, Vietnam*
[5] *Military science Academy, 322 Le Trong Tan street, Dinh Cong, Hoang Mai, Hanoi, 100000, Vietnam*

(Received 13 December 2019; revised manuscript received 2 March 2020; accepted manuscript online 11 March 2020)

Effect of heating time on the structural, morphology, optical, and photocatalytic properties of graphitic carbon nitride (g-C_3N_4) nanosheets prepared at 550 °C in Ar atmosphere is studied. The investigations are carried out by using x-ray diffraction (XRD), scanning electron microscopy (SEM), Fourier-transform infrared spectroscopy (FTIR), UV–vis absorption, and photoluminescence (PL). At a heating temperature of 550 °C, g-C_3N_4 nanocrystals are formed after 0.5 h and become more orderly as the heating time increases. The surface area of the g-C_3N_4 nanosheets significantly increases as the preparation time increases. The g-C_3N_4 prepared in 2.5 h shows the highest photocatalytic performance, decomposing completely 10 ppm RhB solution under xenon lamp irradiation for 2.0 h.

Keywords: nanosheets, photocatalytic, heating time, Ar atmosphere

PACS: 71.20.NR, 71.20.RV **DOI:** 10.1088/1674-1056/ab7e95

1. Introduction

Facing the exhaustion of fossil fuel resources and serious environmental pollution due to industrial and domestic wastes, scientists are actively looking for efficient photocatalysts which can convert solar energy into chemical energy and be used in the photodegradation of environmental pollutants, hydrogen production via water splitting, air treatment, and CO_2 conversion to hydrocarbon fuel.[1–5] In the last few years, graphitic carbon nitride (g-C_3N_4), as a new material, has come into being in this area, and it is a non-metallic semiconductor with a band gap energy of about 2.7 eV ($\lambda \sim 460$ nm), durable, non-toxic, highly recyclable and exhibits superior photocatalytic ability.[2,6–10] Therefore, g-C_3N_4 has become an attractive research object in the field of photocatalyst.

To obtain g-C_3N_4, it is necessary to use carbon and nitrogen-rich precursors such as urea,[11,12] thiourea,[11] melamine,[13,14] cyanamide,[15] dicyandiamide,[16] etc. Common methods for preparing g-C_3N_4 include high-pressure pyrolysis,[17] thermal polymerization,[14] hydrothermal,[18,19] etc. One of the C and N-rich precursors, not expensive and easy to find, is urea. Our previous study showed that with a heating time of 2 h, g-C_3N_4 nanosheets prepared by thermal polymerization in Ar atmosphere at 550 °C exhibited the highest photocatalytic efficiency.[20] In the present work, the heating temperature is fixed at 550 °C while the heating time is changed from 0.5 to 2.5 h to study the effect of the heating time on the formation of crystal structure, optical property, and photocatalytic performance of g-C_3N_4 nanosheets.

2. Experiment

2.1. Preparation of g-C_3N_4

Thermal polymerization in inert Ar atmosphere was adopted to synthesize g-C_3N_4. Firstly, 5 g urea ($\geq$ 97.0%, Sigma-Aldrich) was mixed with ethanol solution, ground for 1 h, and transferred into an alumina crucible. Thermal polymerization process took place at the heating temperature of 550 °C for different time from 0.5 h to 2.5 h in Ar atmosphere by using a tubular furnace. The samples are denoted as CN-x ($x = 0.5$, 1.0, 1.5, 2.0, and 2.5) according to their preparation time.

2.2. Photocatalytic degradation experiment

The 10 ppm Rhodamine B (RhB) solution was used as a reagent to determine the photocatalytic activity of the as-synthesized g-C_3N_4. Initial RhB solution was prepared at a concentration of 20 ppm. As the first step, 0.06 g g-C_3N_4 nanosheets was dispersed in 30 ml distilled water under ultrasonic vibration for 1 h. In the second step, 30 ml g-C_3N_4-containing solution was mixed with 30 ml 20-ppm RhB solution to obtain 60 ml 10-ppm RhB solution containing g-C_3N_4.

*Project supported by the scientific and technological project at the level of Ministry of Education, Vietnam (Grant No. B2018-SPH-06-CTrVL).
†Corresponding author. E-mail: lemaioanh@gmail.com
© 2020 Chinese Physical Society and IOP Publishing Ltd

Firstly, the RhB adsorption experiment was carried out to assess the adsorption ability of g-C_3N_4. The 10 ppm RhB solution containing g-C_3N_4 was stirred in a dark chamber for 30 min to reach an adsorption–desorption equilibrium. The solution was then illuminated by a 300 mW xenon lamp. The xenon lamp was placed at a distance of 6 cm from the surface of the RhB solution. After every 15 min of illumination, an amount of 3 ml of the suspension was taken and centrifuged to remove g-C_3N_4 for UV–vis absorption measurement. The intensity of the 552 nm absorption peak was used to determine the remaining RhB concentration in the solution from which the C/C_0 ratio was calculated.

2.3. Characterizations

The D8 Advance diffractometer (Bruker) with Cu-K_α radiation was used to record the x-ray diffraction (XRD) patterns of the as-synthesized g-C_3N_4 nanosheets. The morphologies of the as-synthesized g-C_3N_4 nanosheets were observed by using a scanning electron microscopy (SEM) (S-4800 NIHE microscope, Hitachi). The Brunauer–Emmett–Teller (BET) surface area was measured by a Micromeritics 3Flex. Ultraviolet–visible (UV–vis) absorption spectra were measured by a Jasco V670 UV–vis spectrophotometer through the diffuse reflectance spectroscopy (DRS) technique for the g-C_3N_4 powder. Fourier transform infrared spectra (FTIR) were measured by an IR Prestige-21 FTIR/NIR spectrometer (Shimadzu). Photoluminescence (PL) spectra were also measured by a fluorescence spectrophotometer (Nanolog iHR 320, Horiba) at the excitation wavelength of 350 nm.

3. Results and discussion

The XRD patterns of the g-C_3N_4 samples prepared at the heating temperature of 550 °C for different time are shown in Fig. 1(a). The samples all exhibit three diffraction peaks located at 12.7°, 24.8°, and 27.5° which are corresponding to the (001), (101), and (002) diffraction planes, respectively. The peak intensity increases as the heating time increases. A comparison between these peaks and the (001), (101), and (002) peaks of standard g-C_3N_4 materials demonstrates that the synthesized g-C_3N_4 is crystallized in hexagonal phase (JCPDS file No. 87-1526). The strongest peak at 27.5° corresponds to the interlayer stacking of the conjugated aromatic system[21] with an interlayer distance of 3.42 Å. It is obvious that as the heating times increase, the (002) peak shifts slightly towards the larger diffraction angle, indicating the narrowing of the interlayer distance and the decrease of crystal parameter c. The calculations show that parameter c decreases from 6.85 Å for CN-0.5 sample to 6.77 Å for CN-2.5 sample (Table 1). The lattice parameter a can be calculated via peak (101) located at 24.8°. The calculations show that parameter a decreases from 4.59 Å to 4.55 Å when the heating time increases from 0.5 h to 2.5 h (Table 1). Parameters a and c varying with the heating time are plotted in Fig. 1(b), which shows that th eg-C_3N_4 crystal is packed more tightly as the processing time increases, similar to what happens as the heating temperature increases.[20] In addition, figure 1(a) shows that the diffraction intensity increases with the peak width narrowing when the heating time increases (Table 1), indicating that the polymerization of g-C_3N_4 takes place more strongly and crystallinity of g-C_3N_4 is higher as the heating time increases. The XRD peak position and peak width change noticeably as the heating time increases from 1.0 h to 1.5 h, which shows that a fairly ordered lattice can be achieved after heating urea at 550 °C for 1.5 h.

Table 1. Peak positions, heights, and full widths at half maximum (FWHM) of (002) XRD peaks, and lattice parameters a and c of as-prepared samples.

Samples	Peak position/(°)	Height	FWHM/(°)	a/Å	c/Å
CN-0.5	27.20	212.06	2.28	4.586	6.846
CN-1.0	27.17	556.71	2.76	4.573	6.842
CN-1.5	27.49	513.75	1.26	4.568	6.805
CN-2.0	27.55	782.80	1.02	4.553	6.779
CN-2.5	27.52	1215.16	1.22	4.545	6.768

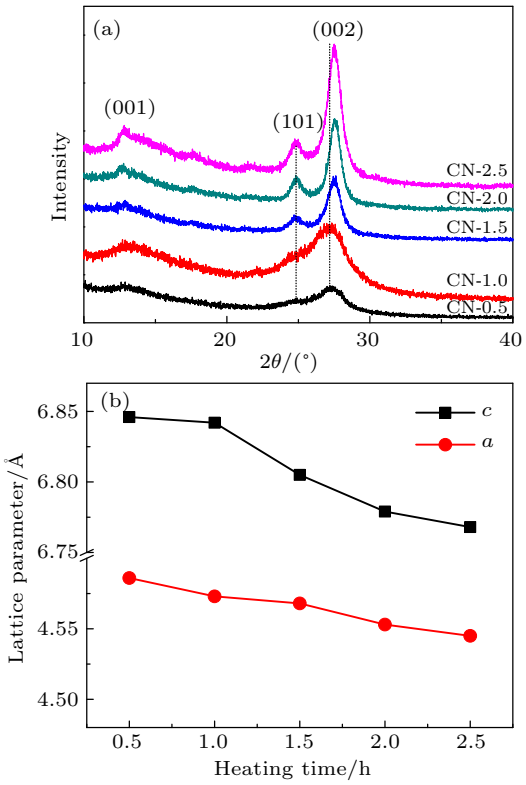


Fig. 1. (a) XRD patterns of g-C_3N_4 samples heated at 550 °C for different heating time and (b) lattice parameters varying with heating time.

Figure 2 shows the infrared absorption spectra of the as-synthesized g-C_3N_4 samples with different heating time. According to the previous studies, the breathing modes of CN heterocycles of triazine units are responsible for the absorption peak at 810 nm while the N–H group substituted into

aromatic primary amine usually shows the stretching absorption in the region of 3000–3600 nm. The stretching mode of the C=N bonds in aromatic rings is responsible for the absorption peak at 1640 cm^{-1} while the stretching modes of the C–N bonds cause some absorption bands in the range of 1200–1500 cm^{-1}. The FTIR spectra of the g-C_3N_4 samples change slightly as the preparation time increases as indicated by the leftward shifting of the peaks 1242 cm^{-1} and 1413 cm^{-1} and the rightward shifting of the peaks 1321 cm^{-1} and 1457 cm^{-1} in Fig. 2(b). In the absorption region of 3000–3600 cm^{-1}, some stretching frequencies are observed at 3084 cm^{-1}, 3162 cm^{-1}, 3269 cm^{-1}, and 3413 cm^{-1}, among which the 3413 cm^{-1} and 3162 cm^{-1} bands can be attributed to asymmetric stretching and symmetric stretching of the NH_2 group while the 3084 cm^{-1} and 3269 cm^{-1} bands are due to the O–H stretching vibrations.[22] It is obviously seen that the 3413 cm^{-1} band shifts gradually toward higher frequency with heating time increasing, consistent with the XRD analysis in which the crystal becomes more ordered and the crystal parameters decrease. In addition, the intensity ratio of 3413 cm^{-1} to 3162 cm^{-1} first increases, and then decreases. This also strengthens the change in crystal structure of g-C_3N_4 as heating time increases.

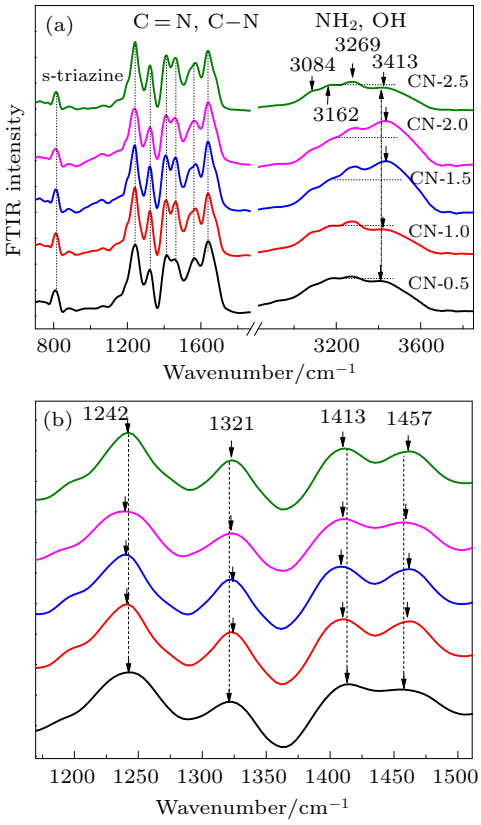


Fig. 2. (a) FTIR spectra of g-C_3N_4 samples prepared at 550 °C with different preparation time and (b) FTIR peak positions varying with wavelength.

The SEM images of g-C_3N_4 synthesized with different heating time are shown in Fig. 3. The g-C_3N_4 sample obtained at 550 °C for 0.5 h in Fig. 3(a) shows heterogeneous particle morphology. Some particles are granular while the others are in the form of nanosheets with a thickness of around 10 nm. When the heating time increases to 1.0 h, the granular particles no longer exist, leaving nanosheets with curved edges. For 1.0 h, the sheets are quite large with very few torn holes on the surface. However, when the heating time increases to 2.0 h and 2.5 h, the samples are still in the form of nanosheets, however, the surfaces of the sheets are punctured or torn into smaller sheets. The g-C_3N_4 obtained at 550 °C for 2.5 h consists of nanosheets that are small in size and more porous than the other samples, which is beneficial for photocatalytic performance due to its large specific surface area.

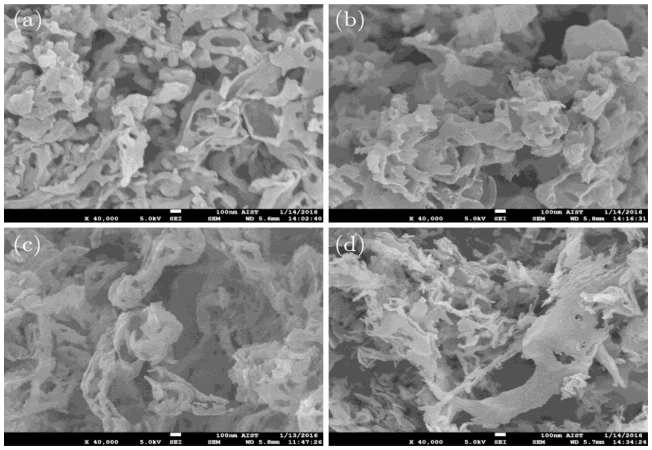


Fig. 3. FE-SEM images of g-C_3N_4 nanosheets synthesized at 550 °C with different preparation time: (a) 0.5 h, (b) 1.0 h, (c) 2.0 h, and (d) 2.5 h.

The BET technique is used to measure the specific surface area and pore size distributions of the as-prepared g-C_3N_4 samples with heating time of 1.0 h, 2.0 h, and 2.5 h as shown in Fig. 4. All samples show type IV isotherms with H3 hysteresis loops, indicating a mesoporous structure that forms slit-shaped pores with a non-uniform size and/or shape. The calculated surface area, average pore volume, and average pore size are listed in Table 2. The surface area of the samples increases from 60 m^2/g to 71 m^2/g and 88 m^2/g for CN-1.0, CN-2.0, and CN-2.5, respectively, which are larger than the specific surface area of pure g-C_3N_4 reported previously.[23,24] This difference is due to the nanosheets being punctured and torn as the heating time increases as seen in the SEM images. All samples exhibit a wide pore size distribution (Fig. 4(b)) and a large average pore width in a range of 10–30 nm.

Table 2. Surface areas, pore volumes, and pore sizes of the as-prepared samples.

Samples	Surface area/$m^2 \cdot g^{-1}$	Pore volume/$cm^3 \cdot g^{-1}$	Pore diameter/Å
CN-1.0	60.0004	0.218945	145.9624
CN-2.0	70.8108	0.426483	240.9142
CN-2.5	87.8561	0.218932	99.6773

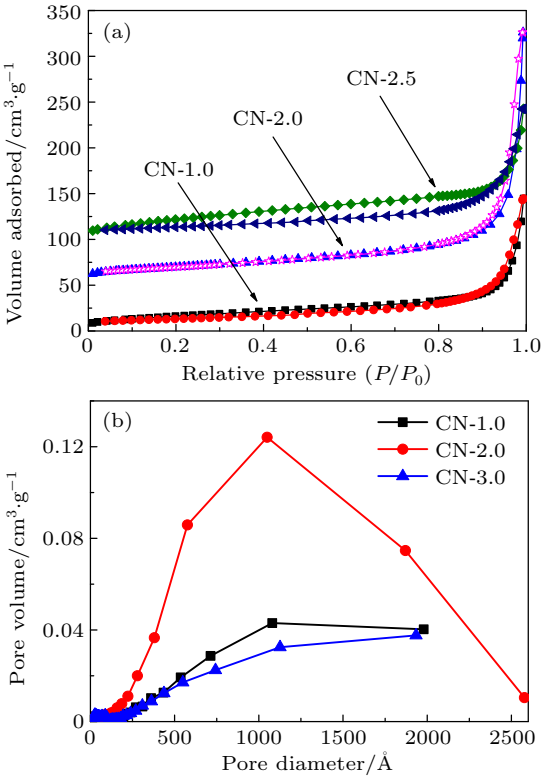


Fig. 4. (a) N_2 adsorption–desorption isotherms of g-C_3N_4 heated for 1.0 h, 2.0 h, and 2.5 h and (b) plots of BJH pore volume versus pore diameter.

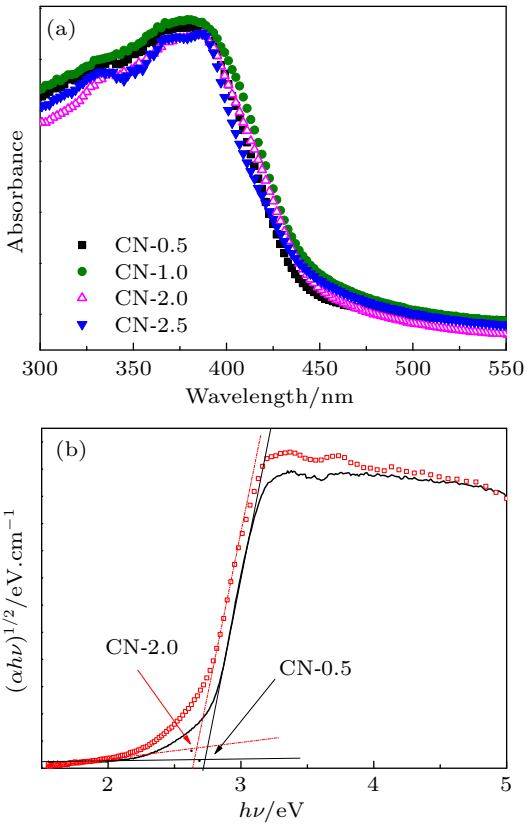


Fig. 5. (a) Absorption spectra of g-C_3N_4 nanosheets obtained at 550 °C with different preparation time and (b) Wood–Tauc method determining band gap energy of indirect semiconductor.

UV–vis diffuse reflectance spectra (DRS) of g-C_3N_4 obtained with different preparation time in Fig. 5(a) indicate an absorption edge at around 450 nm for all samples. It is obvious that the absorption edge first shifts slightly to the right as the heating time increases from 0.5 h to 1.0 h and then inversely shifts to the left with the increasing preparation time. For indirect band gap semiconductor such as g-C_3N_4, ΔE_g can be determined by using Tauc plot of $(\alpha h\nu)^{1/2}$ versus photon energy ($h\nu$) as shown in Fig. 5(b). The band gap is 2.73 eV and 2.66 eV for CN-1.0 and CN-2.0, respectively, revealing that the visible light can be used for exciting photocatalysis.

Figure 6 shows the photoluminescence spectra PL (with excitation wavelength of 350 nm) of the as-synthesized g-C_3N_4 samples with different processing time, indicating a broad blue–green emission band for all samples. The PL band concentrates at 450 nm, in accordance with the UV–vis absorption edge. This PL band can be decomposed into four component peaks as shown in the inset of Fig. 6(a) (for CN-1.5 sample), including P1 (430.4 nm, 2.88 eV), P2 (453.6 nm, 2.73 eV), P3 (491.6 nm, 2.52 eV), and P4 (545.8 nm, 2.27 eV) which accord well with previous reports.[20,25] The PL peaks shift slightly towards the longer wavelength as the processing time increases (see Fig. 6(b)), consistent with the decrease of the energy bandgap obtained in the absorption spectra. In addition, the PL intensity first gradually increases to the highest value at CN-2.0 and then decreases.

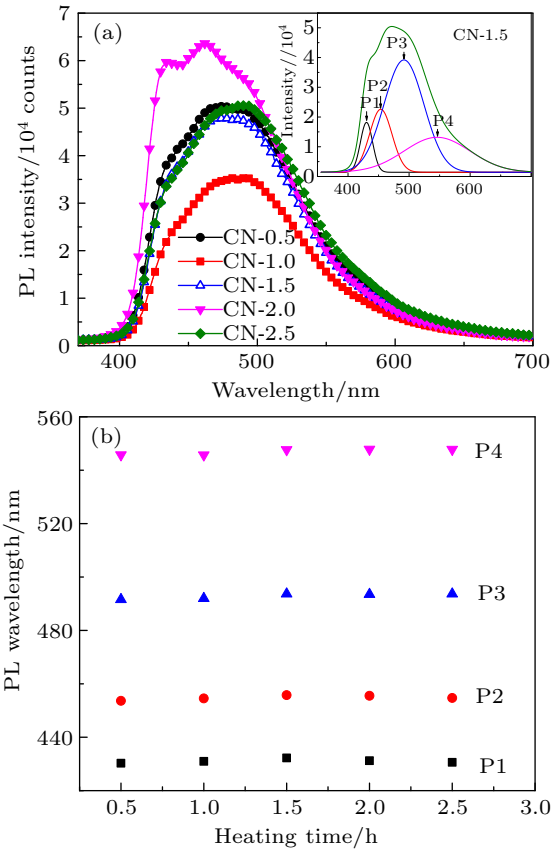


Fig. 6. (a) Photoluminescence spectra of g-C_3N_4 nanosheets obtained at 550 °C with different preparation time, with inset showing the normalized PL spectra and dot lines being Gaussian fitting for CN-2.0 sample, and (b) PL peak positions varying with heating time.

The photocatalytic activity of the g-C_3N_4 sample is assessed through the degradation of Rhodamine B (RhB) solution under the irradiation of xenon lamp in which the UV–vis absorption technique was used to indirectly measure the concentration of remaining RhB. Figure 7 shows the C/C_0 ratio as a function of time, indicating that the RhB degradation highly depends on the heating time. Samples CN-0.5 and CN-1.0 exhibit low photocatalytic efficiency, only about 60% of RhB is degraded after 2 h of exposing. The photocatalytic activity increases sharply as the preparing time increases to 2 h. The CN-2.0 and CN-2.5 degrade almost all RhB after 2 h of exposing. This improvement of photocatalytic performance can be explained by the mesoporous structure of the as-prepared g-C_3N_4 with long heating time. Although CN-2.0 has lower specific surface area than CN-2.5, its pore volume and pore size are both larger, so their photocatalytic performances are almost the same. In addition, the narrower energy band gap of the sample with long processing time also contributes to the improvement of the photocatalytic activity.

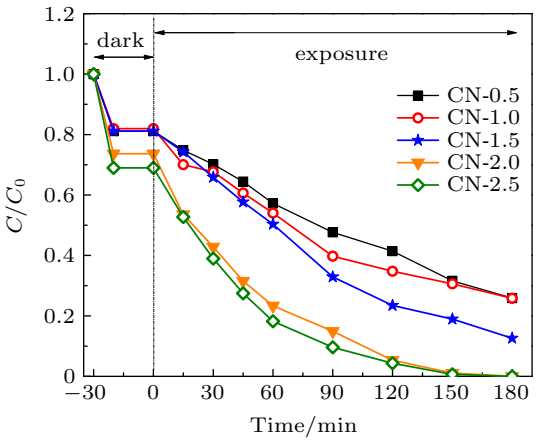


Fig. 7. Adsorption and photocatalytic activities of the g-C_3N_4 prepared at 550 °C with different preparation time in decomposition of RhB solution under xenon lamp irradiation.

4. Conclusion

The structural and physical properties of g-C_3N_4 nanosheets are greatly influenced by the heating time. The crystal lattice is formed more orderly and packed more densely as the heating time increases. The increase in fabrication time also causes the g-C_3N_4 nanosheets to be slightly torn, making them more porous and the specific surface area increase. The energy band gap changes negligibly as the processing time increases. However, the photoluminescence peaks shift slightly toward longer wavelength. The changes in structure, morphology, and physical properties determine the change in the photocatalytic performance of the g-C_3N_4 nanosheets. The g-C_3N_4 nanosheets obtained in long heating time, greater than 2.0 h, possess high photocatalytic activities: the RhB decomposed after 2.0 h of xenon lamp irradiating is accounted for 95%.

References

[1] Gopal N O, Lo H H , Ke T F, *et al.* 2012 *J. Phys. Chem. C* **116** 16191
[2] Kumar S, Karthikeyan S and Lee A 2018 *Catalysts* **8** 74
[3] Bi Y, Ehsan M F, Huang Y, Jin J and He T 2015 *J. CO_2 Utilization* **12** 43
[4] Zhai X, Deng H, Zhou W, Yang P, Chu J and Zheng Z 2015 *Mater. Lett.* **161** 423
[5] Bai X, Wang L and Zhu Y 2012 *ACS Catal.* **2** 2769
[6] Ye S, Wang R, Wu M Z and Yuan Y P 2015 *Appl. Surf. Sci.* **358** 15
[7] Wen J, Xie J, Chen X and Li X 2017 *Appl. Surf. Sci.* **391** 72
[8] Zhang S, Hang N T, Zhang Z, Yue H and Yang W 2017 *Nanomater. (Basel)* **7** 1
[9] Li R, Ren Y, Zhao P, Wang J, Liu J and Zhang Y 2019 *J. Hazard Mater* **365** 606
[10] Wu M, Gong Y, Nie T, *et al.* 2019 *J. Mater. Chem. A* **7** 5324
[11] Dong F, Zhao Z, Xiong T, *et al.* 2013 *ACS Appl. Mater Interfaces* **5** 11392
[12] Xu J, Li Y, Peng S, Lu G and Li S 2013 *Phys. Chem. Chem. Phys.* **15** 7657
[13] Zhang L, Jing D, She X, *et al.* 2014 *J. Mater. Chem. A* **2** 2071
[14] Zhang Y, Pan Q, Chai G, *et al.* 2013 *Sci. Rep.* **3** 1943
[15] Fan X, Xing Z, Shu Z, Zhang L, Wang L and Shi J 2015 *RSC Adv.* **5** 8323
[16] Xu H Y, Wu L C, Zhao H, Jin L G and Qi S Y 2015 *PLoS One* **10** e0142616
[17] Xin G and Meng Y 2013 *J. Chem.* **2013** 1
[18] Ming L, Yue H, Xu L and Chen F 2014 *J. Mater. Chem. A* **2** 19145
[19] Yu X, Yang X and Li G 2018 *J. Electron. Mater.* **47** 672
[20] Mai Oanh L T, Hang L T, Lai N D, *et al.* 2018 *Phys. B: Condens. Matter* **532** 48
[21] Dai H, Gao X, Liu E, *et al.* 2013 *Diamond Relat. Mater.* **38** 109
[22] Rehman Iu, Movasaghi Z, Rehman S 2012 *Vibrational Spectroscopy for Tissue Analysis* (Florida: CRC Press) p. 285
[23] Kesarla M K, Fuentez-Torres M O, Alcudia-Ramos M A, *et al.* 2019 *J. Mater. Res. Technol.* **8** 1628
[24] Shen L, Xing Z, Zou J, *et al.* 2017 *Sci. Rep.* **7** 41978
[25] Yuan Y, Zhang L, Xing J, *et al.* 2015 *Nanoscale* **7** 12343